ACS OMEGA

Article

Cite This: ACS Omega 2019, 4, 13086−13099

http://pubs.acs.org/journal/acsodf

Comparison of α-Helix and β-Sheet Structure Adaptation to a Quantum Dot Geometry: Toward the Identification of an Optimal Motif for a Protein Nanoparticle Cover

Katarzyna Kopeć,[†] Marta Pędziwiatr,[†] Dominik Gront,[‡] Olga Sztatelman,[§] Jakub Sławski,[∥] Magdalena Łazicka,[⊥] Remigiusz Worch,[†] Katarzyna Zawada,[#] Katerina Makarova,[#] Marcin Nyk,[▽] and Joanna Grzyb*[,∥]

[†]Institute of Physics, Polish Academy of Sciences, Aleja Lotników 32/46, PL02668 Warsaw, Poland

[‡]Faculty of Chemistry, University of Warsaw, Pasteura 1, PL02093 Warsaw, Poland

[§]Institute of Biochemistry and Biophysics, Polish Academy of Sciences, Pawińskiego 5a, PL02106 Warsaw, Poland

[∥]Department of Biophysics, Faculty of Biotechnology, University of Wrocław, F. Joliot-Curie Street 14a, PL50383 Wrocław, Poland

[⊥]Department of Metabolic Regulation, Institute of Biochemistry, Faculty of Biology, University of Warsaw, Miecznikowa 1, PL02096 Warsaw, Poland

[#]Department of Physical Chemistry, Faculty of Pharmacy with the Laboratory Medicine Division, The Medical University of Warsaw, Banacha 1 Street, PL02097 Warsaw, Poland

[▽]Advanced Materials Engineering and Modelling Group, Faculty of Chemistry, Wrocław University of Science and Technology, Wybrzeże Wyspiańskiego 27, PL50370 Wrocław, Poland

Supporting Information

ABSTRACT: While quantum dots (QDs) are useful as fluorescent labels, their application in biosciences is limited due to the stability and hydrophobicity of their surface. In this study, we tested two types of proteins for use as a cover for spherical QDs, composed of cadmium selenide. Pumilio homology domain (Puf), which is mostly α-helical, and leucine-rich repeat (LRR) domain, which is rich in β-sheets, were selected to determine if there is a preference for one of these secondary structure types for nanoparticle covers. The protein sequences were optimized to improve their interaction with the surface of QDs. The solubilization of the apoproteins and their assembly with nanoparticles required the application of a detergent, which was removed in subsequent steps. Finally, only the Puf-based cover was successful enough as a QD hydrophilic cover. We showed that a single polypeptide dimer of Puf, PufPuf, can form a cover. We characterized the size and fluorescent properties of the obtained QD:protein assemblies. We showed that the secondary structure of the Puf proteins was not destroyed upon contact with the QDs. We demonstrated that these assemblies do not promote the formation of reactive oxygen species during illumination of the nanoparticles. The data represent advances in the effort to obtain a stable biocompatible cover for QDs.

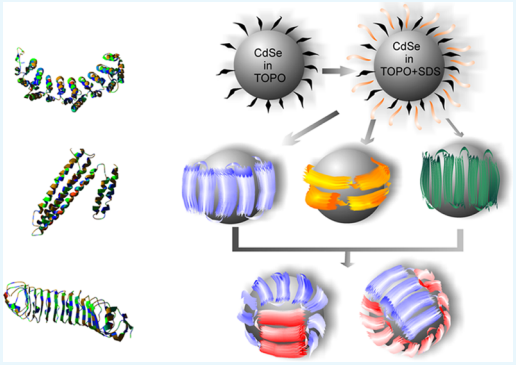

INTRODUCTION

Colloidal quantum dots (QDs) are quasi-spherical nanoparticles with unique fluorescent properties. Currently, they are widely used in several scientific areas, such as medical and life sciences. They are composed of a semiconductor core [e.g., cadmium selenide (CdSe), cadmium telluride (CdTe), or cadmium sulfide (CdS)], an optional semiconductor shell [e.g., zinc sulfide (ZnS)], and an organic passivating crystal surface cover. Although QDs were first identified in materials sciences and electronics,[1] they are now broadly known in life sciences.[2,3] While many potential applications in medicine have been identified, none have yet been commercially successful.[4−7] For medicine and life science applications, QDs may be covered with antibodies or proteins. These additional surface layers may be added to direct QDs to their potential target/therapeutic sites, such as specific organs of the body, the interior of cells, and specific organelles. For this type of application, a QD cover built from long protein chains, as discussed in this paper, may provide additional advantages.

Although QDs are potent fluorophores with a high fluorescence quantum yield, large Stokes shift, and size-tunable emission maximum, their application in a water environment is

Received: April 5, 2019
Accepted: July 23, 2019
Published: August 5, 2019

restricted by their stability and potential toxicity.[8−13] The toxicity of QDs is related mainly to the stability of their organic cover, which protects the core from the removal of Cd ions (or other ions). The ion loss causes defects in the formation of the QD surface and fluorescence bleaching. An organic cover is added to QDs during synthesis, and it is necessary to protect nanoparticles from aggregation.[1] Often, the first cover is composed of hydrophobic hydrocarbons with a functional group (e.g., phosphine, thiol) on one end of the chain. For example, trioctylphosphine (TOP) and trioctylphosphine oxide (TOPO) are used to obtain CdSe and CdSe/ZnS QDs. A phosphine group allows an organic molecule to bind to the nanoparticle atoms. For QDs intended for use in a water environment, the cover must be hydrophilic; this can be realized by oxidation of the hydrophobic cover of hydrocarbons to carboxylic acids or by the substitution of hydrophobic molecules with hydrophilic molecules, such as mercaptopropionic acid or L-cysteine.[14] In most cases, the final cover consists of multiple small molecules. The hydrophilic groups should be charged to prevent aggregation. A carboxylic group or an amine group is also used to enhance the functionalization of the QD, for example, its attachment to antibodies.[3,15]

However, a cover composed of dozens of small molecules can result in the easy loss of individual molecules, followed by the formation of defects on the QD surface. New types of covers may broaden the applications of QDs. In most strategies, there is only one type of functional group available on a QD surface (e.g., a carboxylic group), which reduces the number of groups that can be coupled to it [here, e.g., amino groups by a reaction using 1-ethyl-3-(3-dimethylaminopropyl)-carbodiimide hydrochloride (EDC)]. While this is sufficient for most applications, it may be beneficial to have multiple options. When a protein is used as a QD cover, carboxylic and amine groups are available, but it is also possible to introduce a more complex binding site (e.g., targeting a tetracysteine motif with biarsenical probes or addressing HisTag by Cy3NTA[19]). With one protein working as a QD cover, it is also possible to add a second protein domain that has a different function, for example, being an epitope that can be recognized by specific cell receptors. This may not allow us to simplify the preparation and lead to the ability to control the stoichiometry of nanohybrids.

Recently, we showed the successful use of membrane scaffold proteins (MSPs) when substituting a hydrophobic cover for a hydrophilic cover in CdSe QDs.[20] These nanocrystals, with a diameter of a few nanometers, were made from CdSe, and they were covered with an organic shell composed of TOPO and its derivatives. In the present study, we used CdSe QDs with a diameter of about 3 nm and an emission maximum of 553 nm. The entire procedure, briefly summarized in Figure 1, required a step with detergent to ensure the transient solubilization of the QDs and the stabilization of the MSPs. Several detergents were suitable for that function; however, *n*-octylglucoside was considered to be the most effective one. In the final steps, the detergents were removed by dialysis and gel filtration. The obtained QD:MSP conjugates were monomers (one QD and two to three MSP chains), which were stable for several days. The fluorescent properties of QDs, namely, their emission and extinction spectra, were preserved. However, their quantum yield was decreased; this could be the result of a simple change in a QD surface neighborhood or just the partial lack of a

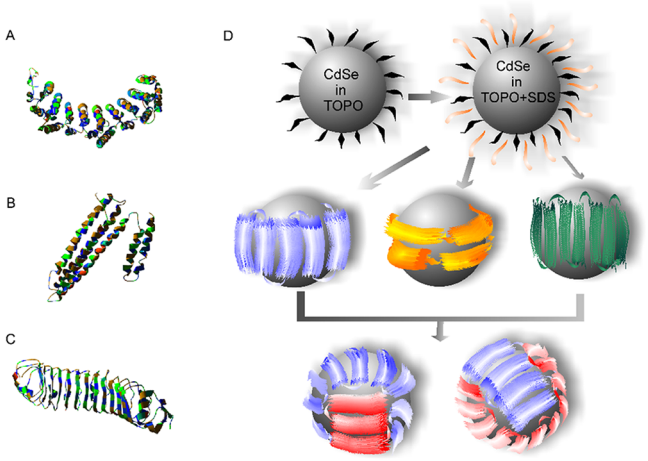

Figure 1. Crystal structures (colored by Kyte and Doolittle[16] hydrophobicity scale: red, basic; brown, acidic; green, polar-noncharged; blue, hydrophobic) of the template proteins considered in the present study: (A) Puf domain (PDB: 3k5q),[17] (B) apolipoprotein A1 (PDB: 2a01),[18] and (C) LRR domain (PDB: 4fmz). (D) Schematic representation of the experiment. Solubilization of hydrophobic QD (CdSe in TOPO) leads to QD in detergent (SDS) micelles or a mixed SDS/TOPO cover. For simplicity, TOPO and SDS were only presented circumferentially; in reality, they cover a sphere. After mixing with Puf, MSP, or LRR, respectively, the QD:protein assemblies were formed. Partial or complete coverage is possible for both Puf and LRR, here presented in two possible projections with two Puf/LRR chains colored in red and violet. The orientation of the protein chains over a sphere are hypothetical based on the crystal structures of Puf/LRR and the known organization of the MSPs in the nanodiscs.

cover. MSPs are derivatives of apolipoprotein A (Figure 1B), and they were first elaborated to support the formation of lipid nanodiscs in vitro.[21,22] Based on the known organization of these proteins in nanodiscs, we proposed that the MSPs encircled the QD sphere, forming a belt. Consequently, they might not be optimal for forming an effective coat on a spherical nanoparticle.

In this study, we addressed whether it is possible to obtain a protein that better adapts to a spherical surface. To the best of our knowledge, there are no natural proteins that are directly able to form a cover for this type of structure that has a sphere with a diameter of a few nanometers. There are basket-like proteins, for example, lipocalins,[23] but these domains bind ligands that are less than 1 nm in diameter. Thus, the type of protein we are looking for must be designed, but designing it from scratch and then improving it, for example, by the random mutation of such a huge structure, are difficult, if not impossible. Therefore, we need more clues for optimal protein elaboration. Toward that end, we addressed the first crucial question: is there a preference for an α-helix motif or a β-sheet motif for proteins that form QD covers? We applied a protein de novo design strategy, namely, in silico mutation, to improve two proteins—a protein with an α-helical structure and a protein with a β-sheet layer—which are similar in shape, size, and hydrophobic pattern but differ in the composition of their secondary structure.

A protein design is a process, which, at first, allowed us to obtain a protein with the desired structure and function.[24−28] Ideally, the design might be created from scratch, with no homology to existing structures. In our approach, due to the

DOI: 10.1021/acsomega.9b00505
ACS Omega 2019, 4, 13086−13099

computational restraints caused by large structures, we had to base the design of known templates. We selected two motifs, the Puf domain and LRR domain, and then we introduced a mutation to improve their fit to the surface of the QDs. Figure 1A,C presents the crystal structures of the selected representatives of the Puf and LRR families. Both protein templates are broad ribbon-like structures known, at least from their crystal structures, to form a shape that might resemble a basket with an internal diameter suitable for accommodating QDs. It is also important to note that the selected proteins are already structural repeats, and it is highly probable that further extension of the motifs will also work. The Puf domain (Figure 1D) is typical for RNA- and DNA-binding proteins, and in nature, it adapts (e.g., to a cleft in the DNA double helix). This motif contains two layers of α-helices. Some proteins have several Puf domain repeats. The LRR domain (Figure 1C) is found in many proteins; it is responsible for forming protein−protein contacts between immunoglobulins and their targets and proteins that are involved in cell adhesion and cytoskeleton formation.[29−31] The LRR domain also consists of two layers; however, one layer is a row of β-sheets (internal), and the other layer is a row of α-helices.

One may intuitively expect that the β-sheet layer would be better for building the desired sphere-wrapped shape since there are many β-barrel proteins, including lipocalins, which bind a ligand inside a protein basket,[23] or toxins, which form pores in the plasma membrane.[32] A β-sheet is flatter, thinner, and generally more flexible than an α-helix.[33,34] However, an α-helix motif is much easier to design, and it has much higher environmental stability than a β-sheet motif.[35,36] Our results suggest that an α-helix structure may be used in future QD covers, and their stability indicates that it will be more useful than β-sheet-based designs. Since the QD geometry suggests that two to three Puf molecules are needed for proper coverage, we also tested the single-chain duplication of a Puf protein, PufPuf. However, we found that such a simple duplication does not improve the stability of the QD:protein assemblies.

RESULTS

Purification Optimization and QD:Protein Assembly Formation. The proteins used in the present study were expressed in *Escherichia coli*. Upon expression in bacteria, both the Puf and LRR proteins were found mainly in the inclusion bodies in all the tested expression conditions. Thus, we decided to purify the proteins under denaturing conditions. The proteins were solubilized completely in 6 M guanidine chloride. We tested refolding by dilution, also in the presence of arginine, but only a small portion of the initial amount of protein was soluble. Finally, we found that, to keep the Puf proteins in the solution, we needed to add a detergent, preferably sodium dodecyl sulfate (SDS). Consequently, we decided to use SDS to solubilize the QDs. This detergent is not easily removed by dialysis, and it is highly probable that some molecules remained in the final QD:protein assembly but in an amount that is not detectable by Fourier transform infrared spectroscopy (FTIR) and that does not influence the secondary structure of proteins. In the present study, pH 8.0 was used because it was more convenient and it corresponded to the pH condition required for possible future applications in in vitro and cell studies. However, QD:protein assemblies could be obtained using a broad pH range (at least 6−9.5; see the description provided in Figure S1, Supporting Information). Hydrophobic CdSe QDs, with TOPO and its derivatives as a cover and an emission maximum at 553 nm, were used in the study. The QD:Puf and QD:PufPuf assemblies were stable for at least 3 months when stored at 4 °C. The stability was estimated from the absorption and emission spectra, which did not change significantly. The QD:LRR preparation was much less stable, as demonstrated by the appearance of a reddish precipitate during storage at the same conditions.

In general, we observed that efficient assembly requires at least 40 μM of protein (and a QD:protein ratio of at least 1:5) when starting the QD:protein mixture. At a higher concentration, the preparation had the same quality. In a lower concentration (not shown), after dialysis, we observed a lower ratio between the QD and the protein absorption and emission. While it was still possible to obtain QD:protein assemblies during the gel filtration, more free protein was observed, and more QD was lost as a precipitate. However, because the assembly process is not a simple binding−unbinding event, it was not possible to analyze the changes in the reaction equilibrium based on the protein concentration. When the QD:Puf assembly or QD:PufPuf assembly was formed, it could be diluted several times; moreover, rechromatography of the fraction caused no changes except for dilution (data not shown). Thus, although binding may occur with a low on-rate constant, the off-rate constant may be close to zero.

Size of the QD:Protein Assemblies. We performed gel filtration to estimate the size of the QD:protein assemblies. As a control, the same experiment was done on the refolded apoproteins that were dialyzed from urea and SDS. As shown in the example chromatograms presented in Figure 2, in all cases, assemblies were formed between the QDs and proteins. The QDs used in the study have radii of 1.43 nm, and theoretically, they should be detectable on the column at elution volumes at about 18−19 mL. However, an elution of QDs alone is not shown because they manifest as a smear over a column, or even as a stack to a column, as very large aggregates. The formation of QD:protein assemblies was characterized by the disappearance of the free protein elution maximum and the appearance of peaks with a shorter elution

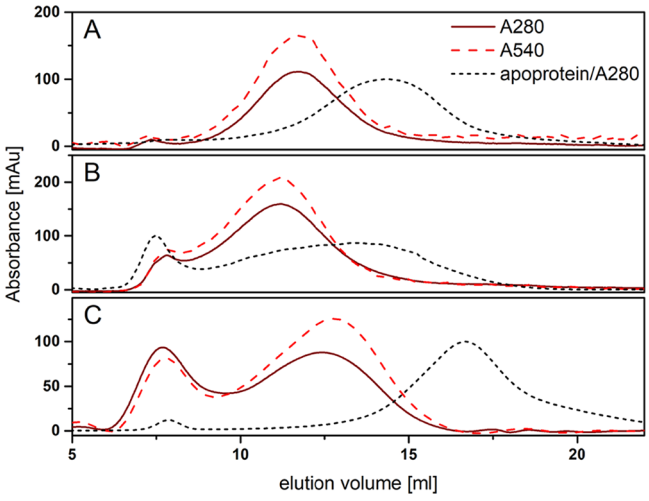

Figure 2. Examples of the elution profiles (gel filtration on Superose 6) of the QD:protein assemblies (followed at 280 and 540 nm) and of the dialyzed apoproteins (followed at 280 nm). (A) QD:Puf, (B) QD:PufPuf, and (C) QD:LRR.

DOI: 10.1021/acsomega.9b00505
ACS Omega 2019, 4, 13086−13099

volume, corresponding to higher Stokes radii: For the QD:Puf assembly, the approximate radii were about 9.7 nm versus 6.4 nm for the apoproteins. For the QD:PufPuf assembly, the apoprotein radii were 10.3 nm versus 6.8 nm, and for the QD:LRR assembly, the apoprotein radii were 8.6 nm versus 3.4 nm. Those species have aligned 280 and 540 nm absorption maxima, which are expected for species containing QDs and proteins. The Stokes radii were calculated on the basis of control run of standards (see the Experimental Section). For the preparation with a higher amount of protein, some peaks of the free proteins, not bound with QDs, were also found (not shown). In some preparations (see Figure 2B,C), higher-mass species corresponding to higher-mass aggregates, eluting at the column void volume (about 7 mL), were present. The number of aggregates was higher for the LRR domain. For QD:Puf and QD:PufPuf, the amount varied between the preparations. We also observed that longer dialysis resulted in a decrease in the amount of aggregates (data not shown), which suggests that some reorganization occurs during that process. We also tested this procedure with the P1D1 protein from the MSP group, for which we already described the formation of the QD:protein conjugates. The results obtained for the QD solubilized with SDS (data not shown) were similar to those shown for the other detergents.

We also analyzed the size of the QD:protein assemblies using fluorescence correlation spectroscopy (FCS). This method shows an average radius of fluorescent molecules in the solution, but it is free of the gel filtration artifacts induced by the interaction with beads. Table 1 presents the hydrodynamic radii of the species obtained during preparation of the QD:protein assemblies, calculated on the basis of the Einstein−Stokes equation. After dialysis, the calculated radii were longer than the radii of the QDs in SDS. Aggregates were also present, which, for the QD:LRR assemblies, render precise calculation impossible. After gel filtration, QD:LRR fractions were immeasurable. For other proteins, the monomer-related fractions were free from aggregates, and the calculated radii were shorter than the radii measured directly after dialysis. The QD:P1D1 radius was even shorter than the radius of the QD in SDS. This finding corresponds to the results obtained in the previous study,[20] and it is most probably caused by the large micelles of the QD:SDS or the partial aggregation of the QDs in SDS.

Table 1. Hydrodynamic Radii Calculated from the FCS Measurement of the QDs Solubilized in SDS and QD:Protein Assemblies after Dialysis and after Gel Filtration (Monomer-Related Fraction)

sample	radius (nm)
theoretical radius[37]	1.43
QD in SDS	5.8 ± 0.2
after dialysis	
QD:P1D1	6.1 ± 0.4
QD:Puf	11.3 ± 0.7
QD:PufPuf	11.8 ± 0.9
QD:LRR	26.8 ± 7.1 (large aggregates)
after gel filtration	
QD:P1D1	4.2 ± 0.2
QD:Puf	7.0 ± 0.6
QD:PufPuf	6.7 ± 0.5
QD:LRR	n.d.

Similar results were obtained for preliminary tests using CdSe/ZnS QDs (data not shown). However, the main problem was the initial solubilization of the CdSe/ZnS QDs, which resulted in a much lower yield of final preparation. Therefore, in subsequent procedures, only CdSe QDs were used.

Electrophoretic Behavior of the QD:Protein Assemblies: An Indication of Size and Stability. The behavior and stability of the QD:protein assemblies were tested using agarose electrophoresis. Figure 3 presents the separation, visualized by the fluorescence of the QDs. The QDs without protein moved faster due to their shorter radius and, possibly, the higher charge provided by the negatively charged SDS molecules. Some of the QDs were stacked in a well, possibly because of losing their SDS micelles. When the protein was present in the assembly, the electrophoretic mobility was lower than that of the free QDs. QD:Puf and QD:PufPuf moved by comparable distances, while P1D1 was faster than QD:Puf but slower than the free QDs. QD:LRR was mostly stacked in a well. Only a small amount of QD:LRR was moving through the gel.

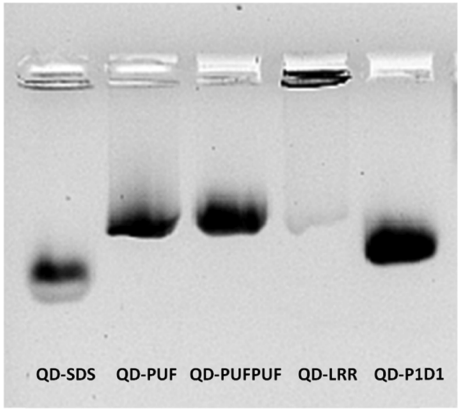

Figure 3. Separation of the QD:protein assemblies on agarose gel with fluorescence visualization. Excitation with a 305 nm trans-illuminator; detection using a CCD camera protected by an EtBr-type broadband filter.

The difference in electrophoretic mobility corresponded (although not directly proportionally) to the zeta (ζ) potential measured for the QDs solubilized in SDS and the QD:protein assemblies (see Figure S2, Supporting Information). The ζ value for the QDs in SDS was at least twice that for the QD:protein assemblies. The specific values of the QD:protein assemblies differed depending on the protein that was used. The value was higher for QD:Puf than for QD:PufPuf, which indicates that the organization of those two proteins on the nanoparticle surface was different. The potential of SDS:QDs (−44.4 mV) was higher than that measured before for SDS-modified CdSe (−57.6 mV[8]). However, in that studies, QDs were much bigger (178 nm) and measured in different buffer conditions, which may influence the measurement. The protein cover of QDs results in an increase in ζ to values corresponding to CdSe QDs with nonionic organic ligands.[8]

Fluorescence Properties: Steady-State Spectra and Fluorescence Lifetime. The maximum emission of the QDs solubilized in SDS was slightly left-shifted in comparison to the organic solvent, from 562 nm in chloroform to 560 nm in SDS-water (Figure 4A). Additionally, the emission intensity

DOI: 10.1021/acsomega.9b00505
ACS Omega 2019, 4, 13086−13099

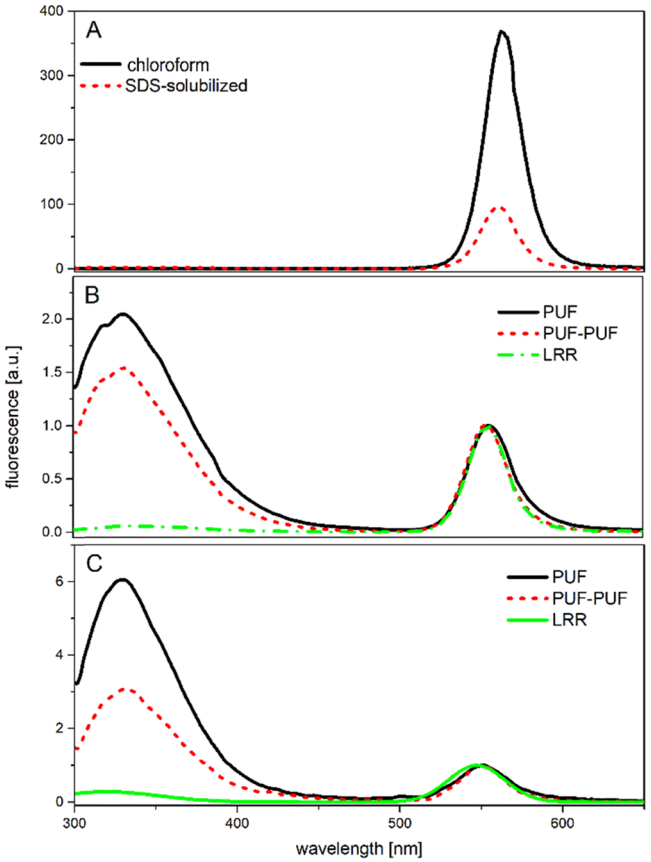

Figure 4. (A, B) Fluorescence spectra (excitation at 280 nm) of the QDs in chloroform and after solubilization in SDS after dialysis in assemblies with proteins (A) and after gel filtration (B) and (C) spectra of monomer-related fractions. The QDs in chloroform and SDS-water in a concentration of 1.5 μM; the other spectra were normalized at the QD emission maximum for easier analysis.

decreased, which corresponded to a fluorescence quantum yield that was about four times lower. For the QD:protein assemblies after dialysis (Figure 4B), the fluorescence emission spectra showed that there were two maxima: at about 330−320 nm (strong emission of the tryptophan residues of Puf and PufPuf and a weak emission of one tryptophan residue and several tyrosine residues of LRR) and at 555 nm for the QDs. After gel filtration, the emission maximum of the QDs was even more left-shifted: to 552 nm for the Puf:PufPuf assembly and to 546 nm for LRR. The protein emission maximum results were the same after dialysis.

During the assembly process, the initial quantum yields of the CdSe QDs (about 9%) were decreased to about 2% for QD:Puf and QD:PufPuf and to about 0.8% for QD:LRR.

The QD fluorescence lifetime was also altered in the QD:protein assemblies (Table 2). Basically, in conjunction with helical proteins, the average fluorescence lifetime was longer by about 2 ns; in contrast, no significant change in the fluorescence lifetime was observed with LRR. Examples of the individual fluorescence decay of QD:SDS and QD:Puf are shown in Figure S3A (Supporting Information).

Table 2. Average Fluorescence Lifetime (τ_{av}) Measured for the QDs Solubilized in SDS and the QD:Protein Assemblies

sample	τ_{av} (ns)
QD in SDS	10.2 ± 0.1
QD:P1D1	13.0 ± 0.1
QD:Puf	12.6 ± 0.2
QD:PufPuf	12.8 ± 0.3
QD:LRR	10.0 ± 0.3

Because the fluorescence decay of QDs is usually multi-exponential,[38] we also analyzed the length of the individual components and the relative ratio of their amplitudes. The best fit was obtained with three components. After assembly with proteins, the lengths of the components and their amplitudes ratio changed (Figure S3B, Supporting Information). In all cases, including LRR, the length of the longest component was increased by at least 2 ns. In all cases, the shortest τ was 0.5−0.6 ns, but its relative contribution increased from about 52% in the QD:SDS assembly to 57% in the assembly with PufPuf, 70% in the LRR and Puf assemblies, and 74% for P1D1.

ATR-FTIR Analysis of the Composition of the QD:Protein Assemblies. Attenuated total reflection FTIR experiment (ATR-FTIR) of the samples was performed to determine the overall composition of the QD:protein assemblies and to evaluate the secondary structure of the proteins. For the overall composition analysis, the main question was as follows: are molecules from the original hydrophobic cover (namely, TOPO and its derivatives[39]) or detergent (SDS) molecules still present in the QD:protein assemblies? All of the analyzed spectra contained a region with absorption due to symmetric and asymmetric stretching of the CH_2 and CH_3 groups and the aliphatic C−H mode (Figure 5A). In a sample containing a protein (shown in the example of the apoPuf and QD:Puf assemblies), there is also an aromatic C−H vibrational mode. We were most interested in determining if there was a change in the relative ratio between the particular vibrational mode intensities when comparing the QD with TOPO on a surface to the apoPuf and QD:Puf. The QD:Puf spectrum was different from the apoPuf spectrum, but the difference was not due to the simple superposition of the QD spectrum and apoPuf spectrum. Especially, the C−H aromatic vibrations and CH_3 symmetric vibrations were relatively intensified. This suggests that the interaction between the QD and protein changes the probability of observing specific vibrations. Moreover, similar changes were found for the QD:PufPuf assembly (data not shown). The analysis of the recorded spectra of QD:protein assemblies did not rule out the possibility that residual TOPO molecules were still present in the assemblies.

The most useful spectral region for examining the presence of TOPO molecules in the assemblies is the 1500−800 cm^{-1} range. Although this region is crowded, some characteristic signals can be observed. Figure 5B presents a comparison of this region for the representative samples obtained from various preparations. In the spectrum of the QD with a hydrophobic cover (original QD preparation, dried from chloroform), we might see the dominant band at 1085 cm^{-1}, which is attributed to the stretching vibration of the P═O group bound to the CdSe surface.[40] There was also a minor signal from a free P═O group (at 1150 cm^{-1} and in the 1500−1350 cm^{-1} region), most likely from the TOPO or TOPO derivatives, as *n*-octyl phosphonic acid[39] molecules are released from the QD during storage. After solubilization with SDS, the mode corresponding to the bound P═O group disappeared, most probably due to masking by the SDS vibrations. There was an absorption in the QD:protein assembly sample at 1134 cm^{-1} and a broad arm at 1085

DOI: 10.1021/acsomega.9b00505
ACS Omega 2019, 4, 13086−13099

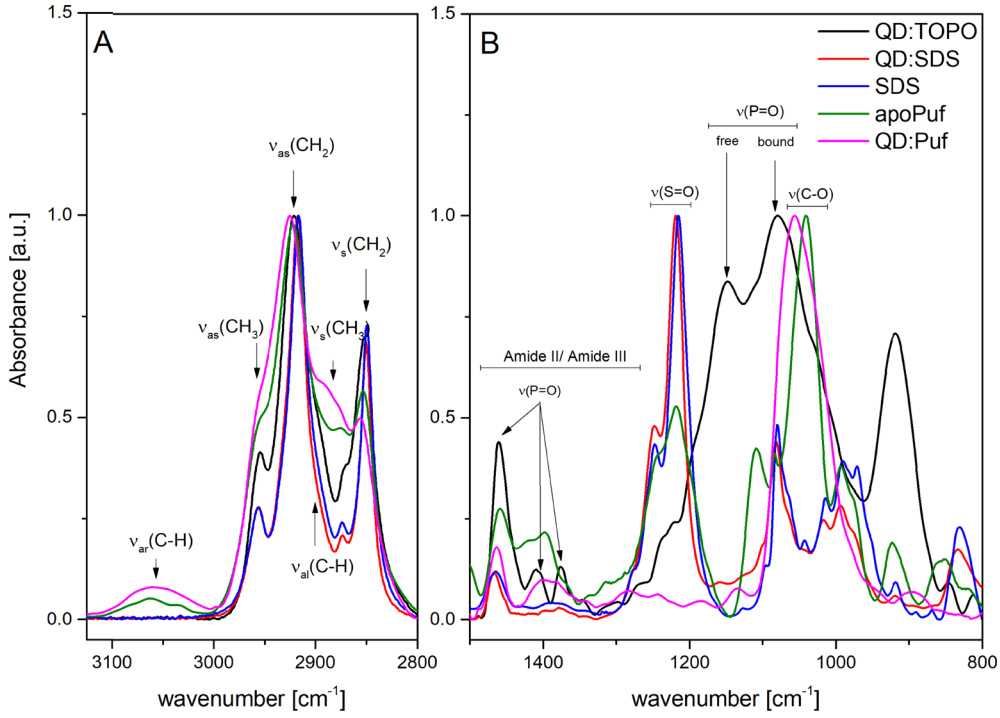

Figure 5. Examples of FTIR spectra in the region of CH_3 and CH_2 symmetric (ν_s) and asymmetric (ν_{as}) stretching vibrations (A) and other fingerprint vibrations and (B) of selected steps in the QD:PufPuf assembly preparation. Spectra were arbitrarily scaled (independently for both regions) to allow for comparison.

cm^{-1}, which may be attributed to the free and bound P═O vibrational modes. This suggests that the original hydrophobic cover molecules were still present in the QD:protein assembly sample. However, in the apoPufPuf sample, minor absorption bands were also observed at those wavelengths. There was no free P═O signature in the QD:protein spectrum in the 1500−1350 cm^{-1} region. Absorption was also seen in this region in the QD:protein sample but with a pattern corresponding more to amide II and amide III modes (in comparison to a free protein) than to the P═O vibrational mode. The comparison of the SDS spectrum and QD:protein assembly spectrum also suggests that all the free SDS molecules were removed during preparation as the S═O stretching mode is missing in this sample. Interestingly, when comparing the apoprotein and QD:protein assembly spectra, a change in the ratio between C−O stretching mode intensity and amide III intensity was observed. It is important to note that the position of the C−O mode was shifted by about 20 cm^{-1} (QD:Puf) or 50 cm^{-1} (QD:PufPuf) in comparison to the apoproteins. These observations do not allow us to draw strict conclusions about the organization of proteins on the QD surface; however, they do prove that a significant amount of protein amino acids was involved in the interaction with the QD surface and energy of the appropriate vibrations was changed.

The secondary structure of the proteins was analyzed from the amide I band in the ATR-FTIR spectra. Figure 6 presents a comparison of amide I for the apoproteins and QD:protein assemblies for Puf, PufPuf, and LRR. The maximum amide I vibration of apoPuf and apoPufPuf were centered at 1650−1660 cm^{-1}, which is the signature of helical structures.[41,42] ApoLRR showed maximum amide I vibration between 1640 and 1650 cm^{-1}, which might suggest the presence of β-structures and an unordered chain. After interacting with the QDs, the maximum for LRR shifted to 1640 cm^{-1},

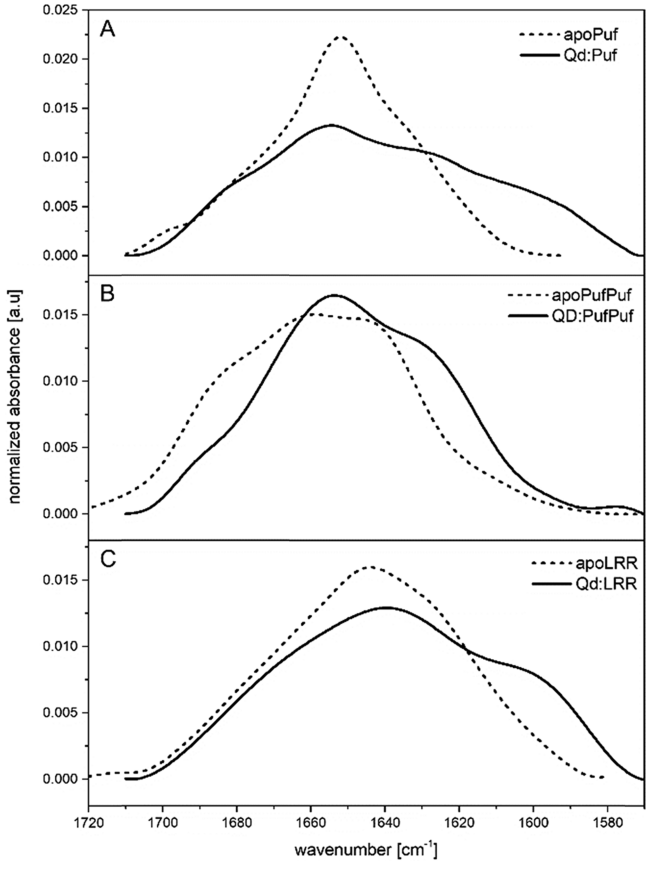

Figure 6. Comparison of the amide I FTIR spectra of the apoproteins and QD:protein assemblies: (A) apoPuf and QD:Puf, (B) apoPufPuf and QD:PufPuf, and (C) apoLRR and QD:LRR. For easier comparison, the area is normalized to 1.

DOI: 10.1021/acsomega.9b00505
ACS Omega 2019, 4, 13086−13099

corresponding to an unordered protein. The Puf and PufPuf assemblies with QDs again showed the amide I maximum corresponding to structures rich in helices; however, the spectrum shape changes, suggesting a reorganization of minor structural features. For QD:Puf and QD:PufPuf, we confirmed the high number of α-helices using circular dichroism measurements (see Figure S4, Supporting Information). For apoPufPuf, the CD spectrum also indicates a mostly helical structure. The main difference between QD:Puf and QD:PufPuf could be due to the higher degree of unordered structure in QD:Puf in comparison to QD:PufPuf. This may be explained by the presence of partially unfolded regions in the terminal parts of the Puf amino acid chain, while in PufPuf (which is simply two Puf molecules on one polypeptide), the average terminus content per amino acid was lower. For the preparation of apoPuf, apoLRR, and QD:LRR, circular dichroism spectra were not reliable to properly assess the secondary structure elements. Detailed analysis of the secondary structure was then possible after the amide I band deconvolution, when the percentage of the area corresponding to the appropriate secondary structure elements may be ascribed to the relative content of this element in a protein structure.[42] The example of a deconvoluted amide I band of apoPufPuf is shown in Figure S5, Supporting Information.

The secondary structure compositions of the studied cases, compared to the values predicted from the design, are summarized in Table 3. Details of the deconvolution of the amide I bands are provided in Table S1, Supporting Information. The secondary structure of the LRR apoprotein corresponds to the design; there is a high amount of β-structure (43%). While α-helix (50%) was found in an amount significantly higher than predicted, that outcome might be easily explained by comparing it to other LRR domains, which also contain a significant amount of helices (for example, in comparison to the NOD-like receptor family[43]). However, after assembly with QDs, we primarily observed an unordered structure with only a small contribution of β-sheets. The opposite behavior was found for Puf and PufPuf. The amount of α-helix in Puf was lower than in the design (45%), with an unexpectedly high number of β-sheets (15%). β-Sheets should not be present in Puf or PufPuf; therefore, this frequency may be attributed to the structures induced by incorrect folding or interaction with the ATR crystal. The β-sheet-like signal should be partially interpreted as arising indirectly from the helices because the interaction between the neighboring helices forms aggregates, which gives a signal in that range (intermolecular β-sheets[41]). After assembly with the QDs, the contribution of the α-helix slightly decreases in Puf (to 39%); it increases to 59% for PufPuf, and the intensity of the bands assigned to the β-sheets/aggregates and unordered structure decreases. This simply means that both Puf and PufPuf are structuralized in the presence of QDs.

Table 3. Comparison of the Relative Content (%) of the Secondary Structure Elements of the Analyzed Proteins and Their Assemblies with QDs, as Deduced from Amide I Deconvolution[a]

protein	% of total		
	α-helix	β-sheet	other
LRR			
designed	12	28	60
apoprotein	50	43	7
QD:protein assembly	0	14	86
Puf			
designed	66	1	33
apoprotein	45	0	55
QD:protein assembly	39	0	61
PufPuf			
designed	66	1	33
apoprotein	37	25	48
QD:protein assembly	59	3	38

[a]The secondary structure element content in designed proteins was calculated from in silico models.

Photogenerated Electron Transfer to Oxygen. Generation of reactive oxygen species (ROS) by QDs is usually a simple test to determine the accessibility of oxygen to the surface of QDs and then the quality of the surface cover. CdSe with the mercaptosuccinic acid cover was shown to generate an ROS, superoxide, and hydroxyl radical.[44] Passivation of the CdSe surface (e.g., by ZnSe) protects it against electron leakage to oxygen.[45] We tested SDS-solubilized QDs and QD:protein assemblies for ROS generation after illumination in the presence of ROS-sensitive spin probe 4-hydroxy-5,5-dimethyl-2-trifluoromethylpyrroline-1-oxide (FDMPO). In a preliminary experiment, performed on water-soluble CdTe QDs, we selected the FDMPO spin probe as the best technique for this application (see the Supporting Information). In that experiment, we observed the spectrum of an FDMPO with an OH radical adduct signal (Figure S6, Supporting Information).[46] When applying the same methodology to the CdSe QDs used in this study, we detected no FDMPO-adduct signal either in the QD:SDS or QD:protein assemblies. This suggests that a QD surface may be protected by a protein coat. A weak, almost isotropic signal with $g \approx 2.06$ (Figure S7, Supporting Information) was present in all the samples without FDMPO. While the signal, most probably resulting from CdSe defects,[47] was almost unchanged during prolonged illumination, it disappeared after the addition of the spin probe.

We also checked the photoinduced electron transfer from the QD to oxygen, directly monitoring the oxygen concentration in a solution using an oxygen electrode. This method does not allow for the identification of which ROS is formed, but it may be more sensitive and allows for monitoring the kinetics of the process. Figure S8 shows the traces recorded during this type of an experiment. Basically, for the same concentration of water-soluble CdTe QDs (control) and CdSe QD:SDS, the oxygen consumption was faster in the QD:SDS suspension. However, for QD:SDS, after about 40 s of illumination, the oxygen consumption stopped; in the CdTe QDs solution, the oxygen consumption was observed for at least 500 s. Additionally, in the CdSe QD:SDS suspension, the occurrence of the second process was noted, leading to the partial recovery of some of the oxygen concentration. The same recovery was detected in the CdTe QDs solution but only when the light was switched off.

For the QD:Puf assembly, no oxygen consumption was observed. For the QD:PufPuf assembly, the oxygen consumption was measurable but at least twice as slow (and two times less efficient in total consumption) than in the QD:SDS solution. Thus, the Puf and PufPuf covers protected the CdSe QDs surface from oxygen. The difference between Puf and PufPuf noted here may provide evidence that independent domains of Puf adapt better to the surface of QDs than the

DOI: 10.1021/acsomega.9b00505
ACS Omega 2019, 4, 13086−13099

double-domain protein PufPuf. This suggests that, in future designs, there should be longer links between the domains to allow for better surface coverage.

DISCUSSION

QDs have a significant potential in biomedical and life sciences as fluorescent labels, as elements of biosensors, and as a source of therapeutic ROS. For researchers working with QDs, one of the serious challenges is ensuring the stability and compatibility of their covers. Compatibility refers to the ability to function in a given environment. In most cases, it also means water solubility (more correctly, water dispersibility). Even if QDs are going to be a source of ROS, the formation of such radicals should be restricted only to the target site. Recently, we proposed a cover based on protein chains composed of MSPs.[20] In the present study, we addressed the issue of the secondary structure composition of proteins dedicated to forming a QD cover. Using a protein as a QD cover, we take advantage of multiple possible reactive groups (carboxyl and amine groups as well as more complex groups, such as tetracysteine or HisTag) as well as the simpler addition of a function to a hybrid by having a second functional protein domain. We wanted to determine if there is any preference between an α-helix and a β-sheet during protein adaptation to the shape of a QD surface. While there are several spherical nanoparticles in living organisms (e.g., blood lipoproteins), there are no structures that have the same size as QDs, with a single peptide cover in vivo, to serve as actual templates. Identifying the answer to our question will enhance our understanding and will be a significant advantage when creating designs for more stable covers in the future. The actual in vitro process of the formation of QD:protein assemblies does not enable high-throughput testing without protein purification. Thus, the random mutation strategy had to be excluded. Thus, as many suggestions as possible are needed from individual studies to design a better protein cover for QDs.

In a previous study, we have shown that α-helical MSPs may work as a cover for QDs, providing reasonable stability in a water solution.[20] The features of MSPs, namely, their length and the amphipathicity of their helices, are ideal for encircling a spherical QD. However, due to geometrical constraints, that type of coating would be composed of a few elements, and it would not equally cover the entire surface of a sphere. This is much better than a coating composed of dozens of tiny thiolic acid molecules, although it may still be an improvement. In this paper, we present another α-helical protein, Puf, that is capable of forming a cover for QDs but with a different spatial arrangement of its helices. We also showed that its duplication, PufPuf, a single-chain version of two Puf proteins, can cover the entire QD surface. We expected the size and other properties of both the QD:Puf and QD:PufPuf assemblies to be virtually the same, which, in most of the tests, was found to be true. We also proved that β-sheet proteins, represented here by LRR, may form a QD cover, but they are much less functional than Puf assemblies.

In this study, we aimed to determine if there were any differences in the way in which Puf or LRR bonded to nanoparticles due to their amino acid composition. Table S2 summarizes the composition of the amino acids on the internal surface of Puf or LRR, in which the side chains may be in contact with the QD surface. To select these residues, we inspected the structures manually, and we selected the residues of the side chains that point to the interior created by the structure curvature. The percentage of the content of the hydrophobic, amphipathic, polar-noncharged, and polar-charged amino acids is similar in both proteins. However, the content of individual amino acids is different. The Puf surface contains 10 Gln residues (19.4%); there is no Gln residue in the putative LRR contact surface. There is more Asn and Thr in the LRR surface. All those amino acids (Gln, Asn, and Thr) are polar-neutral. Gln is a bulkier residue, and intuition dictates that such residues would be a handicap in adapting to a QD surface. LRR is also richer in Tyr (13.4% vs 5.5% in Puf). Residues are found on the edge of the protein structure, and in nature, they are responsible for stabilization of the interaction with RNA and DNA, as well as stabilization of the protein structure. We did not remove the residues; such a motif is present in both Puf and LRR. We also expected that they may help in forming the cover of a QD because aromatic amino acids can form hydrophobic interactions with nanoparticles.[48] No previous experimental or theoretical studies have described specific amino acid interactions with a CdSe surface. However, a molecular dynamic study of amino acids binding to chemically close ZnS is available. Nawrocki and Cieplak[49] calculated the binding energies of natural amino acids placed near the (110) surface of ZnS. These energies are also added to Table S2 for easier comparison. In summary, the total binding energy is 1.7 times higher for Puf than for LRR. Moreover, the average amount of amino acid is 1.6 times higher. Cysteine (Cys) residue is the only amino acid responsible for that difference. Of the initial six Cys residues in Puf, that Cys residue is the only one that cannot be removed in silico without disturbing the stability of the structure. The side chain of this Cys does not point directly to contact with the QD surface; however, with protein flexibility, it can still make contact. Since cysteine is important for Puf structural integrity, and the Puf structure is not destroyed during assembly, we assumed that it is not involved in the binding. If cysteine is not considered, the average binding energy is even higher for LRR.

When the binding energies are analyzed for α-helix- or β-sheet-forming amino acids, the energies vary within the groups, with a general tendency for higher energies for the β-sheet-forming residues and more "surface-neutral" amino acids within the α-helix-forming amino acids. Consequently, we may postulate that a specific amino acid composition is not crucial for binding. The important factor may be the overall surface distribution of the charged residues, as well as the presence of hydrophobic patches. Since the shape, surface, and charge distribution are actually similar for both Puf and LRR, we may assume that the crucial feature is the structural stability of the protein that is in contact with the nanoparticle. We may even postulate that the higher binding energies of the β-sheet-forming amino acids may be a handicap; too strong binding may promote unfolding in the presence of the nanoparticle and then promote aggregation and other unwanted events. While this hypothesis requires additional research to be confirmed, molecular dynamic simulation conducted by Cieplak and co-workers showed a list of small deformations of various proteins near the surfaces of mika,[50] ZnO,[51] ZnS,[49] and gold.[52] The authors did not recognize the differences between α-helical or β-sheet proteins, but they showed the importance of longer contact with the surface, which is mostly formed by the charged residues. Since β-sheet amino acids are more likely to

DOI: 10.1021/acsomega.9b00505
ACS Omega 2019, 4, 13086−13099

form contacts than α-helix-forming amino acids, a structure composed of them may be also more likely to be unfolded.

When MSP wraps a QD, it has to form several threads, such as the way MSPs encircle lipids when forming nanodiscs.[21] Attempting to wrap a QD is the same as trying to use a narrow ribbon to cover a surface of a large ball. The obvious solution is to use a broader ribbon. This cannot be obtained by broadening the α-helix, but it may be created from properly organizing the α-helices or β-sheets. One may imagine that a flat β-sheet would be easier to adapt to the nanoparticle curvature. However, α-helices are more stable than β-sheets. This, with the addition of a suitable amino acid pattern, increases the amphipathicity of the helices, which may overpower the flatness and flexibility advantages of β-sheets. Our research proved the second hypothesis to be true.

Overall, the shapes of LRR and Puf proteins are similar. They have a ribbon-like structure, organized as part of a circle with a broad opening with a 3−4 nm diameter. Moreover, the distribution of the electrostatic charge is similar in both proteins. This may be important when they interact with nanoparticles and other proteins when more than one is necessary to form a cover (compare Figure S9). When comparing the surface area of the proteins, calculated directly from the amino acid distances in the crystal structures, the surface area of PUF is 1331 Å^2, and the surface area of LRR is 918 Å^2. Puf is about 17.2 Å high, and LRR is about 17.9 Å high. The difference in the surface area results from the length of the tape or ribbon formed by the protein structure. The surface area of the QDs used in the present study may be estimated to be 3215 Å^2, which suggests that 2.5 Puf molecules/3.5 LRR molecules are necessary for a complete compact cover. However, due to the side chain of amino acids at the edge of the ribbon, as well as the flexibility of the proteins in the solution, we may assume that two Puf molecules and three LRR molecules are necessary to fully cover a QD sphere. It is known that peptides may help in forming cages for cargo delivery because the flexibility of peptides has been found to help in comprising geometry restrictions.[53,54]

Both the Puf and PufPuf assemblies with QD resulted in nanoparticles with 6.7−7 nm radii. Thus, a protein part adds about 5.5 nm to the dimension of an effective CdSe core, as calculated theoretically. For MSP, as P1D1, the radius was 2.8 nm. A similar value was found previously.[20] This means that, while the cover formed by P1D1 is composed of one layer of helices, Puf and PufPuf have two such layers. This fact is in strong agreement with the initial design. A different organization, namely, protein binding to the QD surface as a coiled coil without an encircling formation, would result in at least a 13 nm difference from the core, as based on the Stokes radii calculated for the apoproteins using gel filtration. Although the average α-helix diameter, measured from crystal structures, is about 0.5 nm (1.5 nm with side chains), the actual value may be a result of a large hydration sphere. Previously, we hypothesized that the difference may be a result of the still present shell of TOPO/phosphonic acid ligand or the detergent molecules. In the present study, we had to use SDS, and it is known that this detergent is difficult to remove completely. One may imagine that SDS molecules will remain between the QD surface and protein. However, both the hydrophobic cover (TOPO or its derivatives) and SDS shell would result in an increase of about 0.8 nm in the radius. Here, the difference in size would demand at least two layers of SDS/TOPO molecules. It would also be detectable by FTIR spectra in a region corresponding to the S═O vibrations of SDS or the P═O vibrations of TOPO. SDS vibrations were not present in the final QD:protein assemblies. Some P═O vibrations may be present but not in the amount corresponding to a shell of molecules.

Our research proves that it is possible to obtain a ribbon-like protein to form a cover of a nanoparticle surface. The design of such a nanoparticle coat has not been addressed until now. In previous studies, some proteins were used only to show the controlled aggregation of nanoparticles.[55,56] Those studies reported on a peptide tag and a tag recognizing protein[55] as well as Zn-mediated homodimeric helix associations.[56] In the present study, a complete protein was not designed from scratch; rather, the adaptation of a protein template served our purpose. The main reason for such a strategy is the lack of force fields to properly describe the interactions between the nonbiological surface of a QD and proteins. Moreover, when designing large proteins, high computing power is required. That is why we decided, at first, to adapt the structures that are already known and that have the probability of forming the desired cover. The Puf proteins bind to a cleft of the DNA double helix. LRR domains also form complexes but with other proteins working as immunoglobulins, hormone receptors, and factors of cell adhesion or cellular trafficking.[29,30] A cover of a QD-like sphere using Puf/LRR requires two molecules to form a basket. While this type of basket is still open, most likely, less of the surface is exposed in comparison to an MSP cover. It is also possible that two to four molecules are needed to create a closed cage, as schematically shown in Figure 1. Our results do not provide enough data to distinguish between hypothetical situations, that is, a basket with a small opening or a closed cage without any opening. The overall stability of the QD:protein assembly, with an extended fluorescence lifetime, suggests that the QD surface is protected from a water environment. The data obtained from the EPR FDMPO spin probe experiment and direct measurement of the photogenerated oxygen consumption by the QDs or the QD:protein assemblies provide additional evidence to support this theory.

LRR motifs are actually known to form a basket-like structure, with an inner diameter of up to 30 Å.[31] More open crystal structures of Puf and LRR are also known. Such proteins, combined in twos or threes, would result in structures with more internal space needed for fitting even larger QDs. The Puf and LRR domains are already multiple repeats of structural motifs, which means that further multiplication would also work. Indeed, the duplication of Puf shown in this paper, resulting in the formation of PufPuf, proves this hypothesis.

Theoretical simulations suggest that, although the CdSe QD shape may be simplified by a sphere, the wurtzite structure of CdSe results in the top, bottom, and side surfaces not being equivalent, with different ligand affinities toward them.[57,58] It has also been shown that affinities of the amino acids varied with different ZnO surfaces.[51] One may then suppose that this influences the binding and orientation of the proteins over the QD surface. While that is possible, this problem demands full atomistic modeling, and it is beyond the current resolution capabilities. Until now, only the behavior of very small proteins near the crystal surface has been successfully modeled.[49] However, the strategy we applied addresses the shape. Moreover, although the phosphine group has a higher affinity toward the polar Se-terminated $(000\bar{1})$ surface, the phosphine

DOI: 10.1021/acsomega.9b00505
ACS Omega 2019, 4, 13086−13099

derivatives (phosphine oxide and phosphonic acid) are more likely to target a nonpolar (1120) and Cd-terminated polar (0001) surface, and all of them can bind to the less-preferred surface. In all the considered cases, the hydrocarbon tails point out, and in subsequent steps, SDS may be uniformly distributed over the surface, obliterating the surface differences. It is still possible that, after removing the detergent, various surfaces will tune protein orientation; however, because several groups may bind to different surfaces with slightly different affinities, it is very unlikely that significant reorganization will occur.

Since there is no amino acid sequence specificity in our proteins toward the CdSe surface, it is also possible that the same proteins might be used as a cover for several other types of nanoparticles, not limited only to semiconductor QDs. Aside from further structural optimization, the next step would be to obtain two-domain proteins, the first domain being a cover, for example, Puf, and the second domain bearing a function, for example, porphyrin (heme, chlorophyll) or an iron−sulfur protein. This will improve the application of QDs and other nanoparticles in several concepts, for example, merging QDs into artificial photosynthesis systems via attachment to photosystems in a mode comparable to platinum ions[59] or visualization of ferredoxin-binding dynamics without impacting its redox state.[38]

CONCLUSIONS

This paper addressed the question of the possibility of forming a QD cover from proteins that differ in the composition of their secondary structures. We used proteins with an α-helix motif (Puf and PufPuf) and a protein with a β-sheet motif (LRR). We found that the α-helices are better than the β-sheets in wrapping QDs, and they may provide a better cover for nanoparticles. The quality of the cover was examined by the oxygen electrode-monitored photogenerated oxygen consumption and the FDMPO spin probe EPR experiment, showing no or much lower ROS generation upon illumination of the samples. We showed that the formed QD:protein assemblies were monomeric, meaning one nanoparticle wrapped by two to three protein chains. We also checked that the Puf/PufPuf secondary structure was not destroyed during the assembly over the QD, but some structuralization occurred. The obtained results provide a set of suggestions for further designs of protein covers for nanoparticles.

EXPERIMENTAL SECTION

Protein Template Selection and in Silico Mutagenesis. *Selection of the Structural Scaffold from Deposits of Puf and LRR Family Members.* Experimental structures from both families were obtained from the Protein Data Bank (PDB) website by searching the website using the PFAM database of[60] protein families, keywords, etc. All the deposits structurally similar to these hits were also selected. In addition, PSI-BLAST searches were performed. More than 200 hits were collected for the LRR domain, and about 50 hits were collected for the Puf family. All these structures were then manually screened to determine their suitability for this project. First, false positives were excluded after careful inspection. After this stage, 35 deposits for the Puf domain and 137 for the LRR domain were recorded. These were further inspected based on the geometry of the inner surface, for example, the area, the radius of curvature, and the number of repeats. Finally, chain A of 4fmz (an internalin from *Listeria monocytogenes*) deposit was selected as the model structure of the LRR domain; chain A of 3k5q (*Caenorhabditis elegans* fem-3 binding factor[17]) was selected as the model structure of the Puf domain.

Mutation Design. For each of the two selected proteins, multiple sequence alignment (MSA) was computed from sequences found by PSI-BLAST using MUSCLE.[61] Moreover, maps of the structural interactions (e.g., contacts, hydrogen bonds) were calculated using the BioShell[62,63] toolkit. These two sources of data were used to plan the mutations to be placed on the inner side of the protein, so it would more likely accommodate a QD. The structures of a mutated protein were calculated using the RosettaScripts[64] application of the Rosetta[65] suite. During the modeling process, each mutated side chain was subjected to energy minimization, together with its 8 Å spherical neighborhood, using the Talaris 2014 force field. All the residues (both the backbone and their side chains) that were located further than 8 Å from any mutated position remained fixed during the modeling to prevent the protein from changing its global shape (e.g., its curvature radius).

The following mutations were introduced to 3k5q (Puf domain): K163A, K124A, R121V, R197V, K163V, K124V, R121A, R197A, C136S, C37S, C114A, C190S, C238V, and C266A.

The following mutations were introduced to 4fmz (LRR domain): E66A, K90A, G93A, L112A, T115C, T160C, L223G, T243V, and L310A.

Protein Genes, Expression, and Purification. Genes corresponding to the designed amino acid sequences of Puf and LRR were ordered from Invitrogen Ltd. Sequences were optimized for expression in *E. coli* and cloned into the *Nco*I/*Xho*I restriction sites of the pet28 vector. The C-terminal HisTag present in a vector was also preserved for future purification processes. The *PufPuf* gene was constructed from the *Puf* gene by duplication. To create a construct coding for the double PUF, the *PUF* sequence was amplified using polymerase chain reaction (PCR) with primers PP_for and PP_rev containing additional restriction sites (*Xho*I and *Bam*HI), using Phusion polymerase (Thermo Scientific), according to the manufacturer's instruction, and 25 cycles (98 °C for 10 s, 50 °C for 15 s, and 72 °C for 30 s). The following primer sequences were used: TACGGGATCCCTGCCGACGTGGTCCCTGGATTCTA (PP_for) and TCAGCTCGAGTTACGAACGCAGGTTTGCCAGGGTTT (PP_rev).

The PCR product was inserted into a pJET2.1 vector using T4 ligase (Thermo Scientific) and the protocol for blunt end ligation. pET-PUF and pJET2.1-PUF were digested with Fast Digest *Bam*HI and *Xho*I enzymes (Thermo Scientific). The enzymes were inactivated by heating at 85 °C for 15 min; *Puf* was separated from the vector using agarose electrophoresis, followed by band excision and DNA purification using GeneJET Gel Extraction and DNA Cleanup Micro Kit (Thermo Scientific). The digested pET-Puf and Puf were ligated together using T4 ligase (Thermo Scientific). Bacterial colonies containing ligated vectors were selected using rapid disruption of bacterial colonies followed by agarose electrophoresis to test the size of the plasmids. The identity of the plasmids was verified using restriction analysis and confirmed by sequencing.

Vectors were transformed into BL21(DE3) *E. coli* under kanamycin selection. Bacteria were grown in lysogeny broth

DOI: 10.1021/acsomega.9b00505
ACS Omega 2019, 4, 13086−13099

(LB) with 50 μg/mL kanamycin at 37 °C until OD = 0.6−0.8 was reached. Protein production was induced by 1 mM IPTG (isopropyl β-D-1-thiogalactopyranoside) and grown for an additional 3 h at 37 °C. The proteins were then purified from the inclusion bodies. Basically, a bacterial pellet was resuspended in 25 mM Tris/HCl buffer (pH 8.0) containing 100 mM NaCl and DNase I (10 μg/mL), disrupted by sonication (5 min of 10 s on/off pulses), and centrifuged again. The resulting pellet was washed with the buffer containing 1% Triton X-100 and then with the buffer without additions. Finally, the pure inclusion bodies were dissolved in 8 M guanidinium chloride (GuaHCl). Complete dissolving required at least 8 h of incubation with gentle heating (36−42 °C). The dissolved proteins were stored frozen in aliquots for further use. Prior to assembly, GuaHCl was removed by dialysis for 48 h. It was also necessary to add 1% SDS (final concentration) to the GuaHCl-solubilized protein solution prior to dialysis. If no detergent was present, most of the preparation precipitated. Several detergents were tested, and SDS was found to be optimal for this experiment. The pure proteins were about 46 and 38 kDa, with a 280 nm theoretical extinction coefficient of 33,640 and 20,400 M^{-1} cm^{-1} for Puf and LRR, respectively.

Preparation of the QDs. The synthesis of the TOPO-capped CdSe hydrophobic QDs was conducted as described recently.[20] The morphology of the raw QDs was studied using transmission electron microscopy (TEM) on an FEI Tecnai G^2 20 X-TWIN microscope. The absorbance was recorded with a JASCO V670 spectrometer. Figure S10A shows the representative TEM/high-resolution TEM (HRTEM) micrographs of the CdSe QDs, proving their spherical shapes and the uniformity of their morphology. The CdSe particle size analysis (Figure S10B) of 50 particles using several low-resolution TEM micrographs indicated that the average particle size was 3.2 nm, with a standard deviation of 0.4 nm. Analysis of the HRTEM micrographs of the QDs clearly indicates that the sample contains crystalline particles. The 3.51 Å lattice fringes observed in the HRTEM micrograph (inset in Figure S10A) correspond to (002) lattice planes of hexagonal CdSe. The selected-area electron diffraction (SAED) pattern of the particles (Figure S10C) could be indexed to the (002) corresponding (*hkl*) planes of the standard hexagonal CdSe structure. Figure S10D presents the energy-dispersive X-ray (EDX) spectrum of the as-prepared CdSe QDs. The characteristic peaks of Cd and Se indicate that the obtained particles are indeed the CdSe compound. Additional peaks marked as O, P, and Cu are due to oxide, phosphor, and copper, respectively, which come from the copper grid used in the TEM sampling and the TOPO surfactant used during the synthesis of CdSe QDs. The average size of the QDs was calculated from the position of the absorption maximum using expressions derived by Yu et al.[37] The absorption spectra of the raw CdSe QDs dissolved in chloroform with the first exciton absorption maximum at 553 nm are shown in Figure S1. This allows us to estimate the average diameter of the particles as about 3.1 ± 0.2 nm.

Preparation of the QD:Protein Assemblies. The QDs were solubilized in SDS, as described previously.[20] The QD:protein assemblies were formed by mixing the solubilized QDs with proteins (prepared as described above) in a QD:protein ratio of 1:5 or higher. This preparation was dialyzed against 25 mM Tris/HCl with 100 mM NaCl for at least 36 h, with several buffer changes. Finally, the QD:protein assemblies were separated from the aggregates and the excess of protein or the free SDS molecules using gel filtration on Superose 6 (GE Healthcare) column.

Steady-State Spectral Analysis. The ultraviolet/visible (UV/VIS) absorption spectra were recorded with the Cary 50Bio spectrophotometer in the 250−800 nm range, with 1 nm resolution. Quartz cuvettes with an optical pathway of 1 cm or 4 mm were used, depending on the sample concentration.

Steady-state fluorescence spectra were recorded with the Cary Eclipse spectrofluorometer. In most of the presented results, a 280 nm λ excitation wavelength was used. Slits and sensitivity were adjusted to optimize the signal-to-noise ratio. Usually, 5 nm emission and 5 nm excitation slits and medium sensitivity were used.

The fluorescence quantum yield was calculated using a comparative method,[66] with AlexaFluor488 (Q_y = 0.92[67]) as a reference.

Gel Filtration. For size exclusion columns, Superdex 200 5/150 (GE Healthcare) for small-volume samples or Superose 6 10/300 (GE Healthcare) for larger sample volumes was connected to the Akta Purifier (GE Healthcare) chromatographic system. Elution was performed using the parameters recommended for each column. Samples were loaded with a 100 μL or 1 mL loop. Elution was analyzed spectrophotometrically, simultaneously at two wavelengths (280 and 540 nm). For purification purposes and further analysis, fractions of 0.5−1 mL were collected with an automatic fraction collector. Stokes radii were calculated based on the calibration curve, which was obtained by a separate run of protein standards of known radii (HMW calibration kit, GE Healthcare).

Agarose Electrophoresis. Agarose gels (0.8% ClearView Agarose, BioS&T, Canada) were prepared and run with 25 mM Tris/HCl (pH 8.0) buffer in a typical horizontal electrophoretic system. The samples were mixed with glycerol to a final concentration of 20% prior to loading on the gel. The fluorescent signal of the QDs was used for visualization with ChemiDoc (BioRad). The gels were placed directly on the transilluminator, and fluorescence was excited with 302 nm wavelength. A signal was recorded using a CCD camera, protected by an EtBr-type broadband filter.

Zeta Potential Determination. Zeta potential was measured using ZetaSizer Nano ZS, Malvern. Data were analyzed using Malvern software.

Fluorescence Lifetime Measurements. Fluorescence lifetime measurements were performed using the Zeiss LSM710 microscope with an LSM upgrade kit (PicoQuant, Berlin, Germany), as previously described,[68] with the detection range optimized for currently used QDs.

Fluorescence Correlation Spectroscopy (FCS). FCS measurements were performed on a Zeiss 780 ConfoCor 3 microscope with a C-Apochromat 40×, numerical aperture (NA) 1.2 water immersion objective at room temperature (24.0 ± 0.3 °C), with Alexa Fluor 488 (Thermo Fisher Scientific, USA) as a standard. Experimental details were previously described in ref 69, with the detection range optimized to cover the emission range of the QDs. Hydrodynamic radii were calculated based on the Stoke−Einstein equation, as described in ref 69.

Attenuated Total Reflection (ATR) Fourier-Transformed Infrared Spectroscopy (FTIR). For the ATR-FTIR analysis, the apoproteins and QD:protein assemblies were deposited (10−15 μL drop) and partially dried on a clean

DOI: 10.1021/acsomega.9b00505
ACS Omega 2019, 4, 13086−13099

gold surface to obtain a hydrated film. Prior to analysis, the protein samples were subjected to a buffer exchange to D_2O on PD SpinTrap G-25 columns (GE Healthcare). The spectra were recorded with a Nicolet iS10 FT-IR spectrometer (Thermo Fisher) working in ATR mode in the range of 4000−750 cm^{-1} and 1 cm^{-1} resolution, and 30 spectra were averaged. Amide I analysis was performed using OriginPro 9 software (OriginLab Corporation, USA).

Electron Paramagnetic Resonance Spectroscopy. Electron paramagnetic resonance (EPR) spectroscopy experiments were performed both in the presence and in the absence of an FDMPO spin trap. The EPR spectra were registered with a MiniScope200 X-band spectrometer (Magnettech) at room temperature using a flat quartz cell. The following parameters were used: central field, 331 mT; sweep range, 10 mT; sweep time, 30 s; four scans; microwave power, 6.3 mW; modulation amplitude, 0.1 mT. Simulations were performed using the "garlic" function in the EasySpin toolbox in MATLAB.[70] The QD or QD:protein samples were mixed prior to the experiment with a small aliquot of 10 mM ethanol stock solution FDMPO to obtain a final concentration of 50 μM. The illumination experiment was performed by placing samples in an EPR quartz cuvette, placed 1 cm next to an 8 W UV bulb (305 nm maximum emission), protected additionally by a UG-11 bandpass filter (Schott, Germany).

Photoinduced Oxygen Consumption. Photoinduced oxygen consumption by the QD solution was measured with an oxygen electrode (Oxygraph+ apparatus, Hansatech Ltd., UK) connected to a computer. The measurement chamber was stabilized at 22 °C by a 1 cm-thick water jacket connected to a circulating water bath. A sample was illuminated by a KL 1500 white light source (Zeiss GmbH) using its fiber light guide arm placed at the water jacket wall. The estimated light intensity inside the measuring chamber was 2000 μE.

■ ASSOCIATED CONTENT

Supporting Information

The Supporting Information is available free of charge on the ACS Publications website at DOI: 10.1021/acsomega.9b00505.

Results of zeta potential measurements, examples of the fluorescence decays, comparison of amide I of ATR-FTIR spectra deconvolution results, circular dichroism spectra of the apoproteins and the QD:protein assemblies, example of the amide I band deconvolution, CW-EPR spectra for the illuminated CdTe QD in the presence of FDMPO and QD:Puf without FDMPO, example traces illustrating the light-induced oxygen consumption by the QDs and QD:protein assemblies, and detailed characteristics of the raw QDs (PDF)

■ AUTHOR INFORMATION

Corresponding Author

*E-mail: joanna.grzyb@uwr.edu.pl.

ORCID

Marcin Nyk: 0000-0002-0329-4038

Joanna Grzyb: 0000-0002-7305-9471

Author Contributions

K.K. and M.P. optimized the protein expression and purification, optimized the preparation of the QD:protein assemblies, performed the gel filtration experiments, agarose electrophoresis, UV/VIS, and fluorescence steady-state measurements, and prepared the samples for the other techniques. D.G. designed the Puf and LRR. O.S. prepared the *Puf Puf* gene. J.S. performed the CD measurement. R.W. performed the FCS and fluorescence lifetime measurements and analyzed the data. M.Ł. performed the FTIR experiment and participated in the FTIR data analysis. M.N. prepared the initial QDs. K.Z. and K.K. performed the EPR measurement. K.M. performed the EPR data simulation. J.G. designed the study, participated in the data analysis, and wrote the manuscript draft. All the authors participated in the final manuscript preparation and revision.

Notes

The authors declare no competing financial interest.

■ ACKNOWLEDGMENTS

This research study was financially supported by a grant from the National Centre for Research and Development (Lider/012/445/L-4/12/NCBR/2013) and a Sonata Bis grant from the National Science Centre, Poland (UMO-2016/22/E/NZ1/00673). Protein preparation, gel filtration, FCS, and fluorescence lifetime measurements were partially performed in the laboratories of NanoFun (POIG.02.02.00-00-025/09). The authors are grateful to Paweł Osewski (CENT, UW, Warsaw) for his assistance in the FTIR measurement and to Anna Dąbrowska (Institute of Physics, PAS, Warsaw) for her participation in initial phases of the Puf purification and LRR design. Prof. Jerzy Gubernator and Mr. Adam Markowski (Department of Lipid and Liposomes, University of Wrocław) are acknowledged for access to Zetasizer and assistance in measurements.

■ REFERENCES

(1) Pu, Y.; Cai, F.; Wang, D.; Wang, J.-X.; Chen, J.-F. Colloidal Synthesis of Semiconductor Quantum Dots toward Large-Scale Production: A Review. *Ind. Eng. Chem. Res.* **2018**, *57*, 1790−1802.

(2) Ghasemi, Y.; Peymani, P.; Afifi, S. Quantum dot: magic nanoparticle for imaging, detection and targeting. *Acta Biomed.* **2009**, *80*, 156−165.

(3) Schiffman, J. D.; Balakrishna, R. G. Quantum Dots as Fluorescent Probes: Synthesis, Surface Chemistry, Energy Transfer Mechanisms, and Applications. *Sens. Actuators, B* **2018**, *258*, 1191−1214.

(4) Kowalik, P.; Elbaum, D.; Mikulski, J.; Fronc, K.; Kamińska, I.; Morais, P. C.; De Souza, P. E.; Nunes, R. B.; Veiga-Souza, F. H.; Gruzeł, G. Upconversion fluorescence imaging of HeLa cells using ROS generating SiO 2-coated lanthanide-doped NaYF 4 nano-constructs. *RSC Adv.* **2017**, *7*, 30262−30273.

(5) Park, Y.; Ryu, Y. M.; Wang, T.; Jung, Y.; Kim, S.; Hwang, S.; Park, J.; Bae, D. J.; Kim, J.; Moon, H. Tumor Imaging: Colorectal Cancer Diagnosis Using Enzyme-Sensitive Ratiometric Fluorescence Dye and Antibody−Quantum Dot Conjugates for Multiplexed Detection (Adv. Funct. Mater. 4/2018). *Adv. Funct. Mater.* **2018**, *28*, 1870026.

(6) Hassan, M.; Gomes, V. G.; Dehghani, A.; Ardekani, S. M. Engineering carbon quantum dots for photomediated theranostics. *Nano Res.* **2018**, *11*, 1−41.

(7) Lee, J. S.; Youn, Y. H.; Kwon, I. K.; Ko, N. R. Recent advances in quantum dots for biomedical applications. *J. Pharm. Invest.* **2018**, *48*, 209−214.

(8) Guo, G.; Liu, W.; Liang, J.; He, Z.; Xu, H.; Yang, X. Probing the cytotoxicity of CdSe quantum dots with surface modification. *Mater. Lett.* **2007**, *61*, 1641−1644.

(9) Hardman, R. A Toxicologic Review of Quantum Dots: Toxicity Depends on Physicochemical and Environmental Factors. *Environ. Health Perspect.* **2006**, *114*, 165−172.

DOI: 10.1021/acsomega.9b00505
ACS Omega 2019, 4, 13086−13099

(10) Lovrić, J.; Cho, S. J.; Winnik, F. M.; Maysinger, D. Unmodified cadmium telluride quantum dots induce reactive oxygen species formation leading to multiple organelle damage and cell death. *Chem. Biol.* **2005**, *12*, 1227−34.
(11) Zhang, L. W.; Monteiro-Riviere, N. A. Mechanisms of quantum dot nanoparticle cellular uptake. *Toxicol. Sci.* **2009**, *110*, 138−155.
(12) Modlitbová, P.; Novotný, K.; Pořízka, P.; Klus, J.; Lubal, P.; Zlámalová-Gargošová, H.; Kaiser, J. Comparative investigation of toxicity and bioaccumulation of Cd-based quantum dots and Cd salt in freshwater plant Lemna minor L. *Ecotoxicol. Environ. Saf.* **2018**, *147*, 334−341.
(13) Modlitbová, P.; Pořízka, P.; Novotný, K.; Drbohlavová, J.; Chamradová, I.; Farka, Z.; Zlámalová-Gargošová, H.; Romih, T.; Kaiser, J. Short-term assessment of cadmium toxicity and uptake from different types of Cd-based Quantum Dots in the model plant Allium cepa L. *Ecotoxicol. Environ. Saf.* **2018**, *153*, 23−31.
(14) Sajwan, R. K.; Bagbi, Y.; Sharma, P.; Solanki, P. R. L-cysteine and 3-mercaptopropionic acid capped cadmium selenide quantum dots based metal ion probes. *J. Lumin.* **2017**, *187*, 126−132.
(15) Tsuboi, S.; Sasaki, A.; Sakata, T.; Yasuda, H.; Jin, T. Immunoglobulin binding (B1) domain mediated antibody conjugation to quantum dots for in vitro and in vivo molecular imaging. *Chem. Commun.* **2017**, *53*, 9450−9453.
(16) Kyte, J.; Doolittle, R. F. A simple method for displaying the hydropathic character of a protein. *J. Mol. Biol.* **1982**, *157*, 105−132.
(17) Wang, Y.; Opperman, L.; Wickens, M.; Hall, T. M. T. Structural basis for specific recognition of multiple mRNA targets by a PUF regulatory protein. *Proc. Natl. Acad. Sci. U. S. A.* **2009**, *106*, 20186−20191.
(18) Ajees, A. A.; Anantharamaiah, G. M.; Mishra, V. K.; Hussain, M. M.; Murthy, H. K. Crystal structure of human apolipoprotein A-I: insights into its protective effect against cardiovascular diseases. *Proc. Natl. Acad. Sci. U. S. A.* **2006**, *103*, 2126−2131.
(19) Fessenden, J. D.; Mahalingam, M. Site-specific labeling of the type 1 ryanodine receptor using biarsenical fluorophores targeted to engineered tetracysteine motifs. *PLoS One* **2013**, *8*, No. e64686.
(20) Dąbrowska, A.; Nyk, M.; Worch, R.; Grzyb, J. Hydrophilic colloidal quantum dots with long peptide chain coats. *Colloids Surf., B* **2016**, *145*, 662−670.
(21) Bayburt, T. H.; Grinkova, Y. V.; Sligar, S. G. Self-assembly of discoidal phospholipid bilayer nanoparticles with membrane scaffold proteins. *Nano Lett.* **2002**, *2*, 853−856.
(22) Bayburt, T. H.; Sligar, S. G. Membrane protein assembly into Nanodiscs. *FEBS Lett.* **2010**, *584*, 1721−1727.
(23) Grzyb, J.; Latowski, D.; Strzałka, K. Lipocalins−a family portrait. *J. Plant Physiol.* **2006**, *163*, 895−915.
(24) Bryson, J. W.; Betz, S. F.; Lu, H. S.; Suich, D. J.; Zhou, H. X.; O'neil, K. T.; DeGrado, W. F. Protein design: a hierarchic approach. *Science* **1995**, *270*, 935−941.
(25) Calhoun, J. R.; Kono, H.; Lahr, S.; Wang, W.; DeGrado, W. F.; Saven, J. G. Computational design and characterization of a monomeric helical dinuclear metalloprotein. *J. Mol. Biol.* **2003**, *334*, 1101−1115.
(26) Chevalier, A.; Silva, D.-A.; Rocklin, G. J.; Hicks, D. R.; Vergara, R.; Murapa, P.; Bernard, S. M.; Zhang, L.; Lam, K.-H.; Yao, G.; Bahl, C. D. Massively parallel de novo protein design for targeted therapeutics. *Nature* **2017**, *550*, 74.
(27) Khoury, G. A.; Smadbeck, J.; Kieslich, C. A.; Floudas, C. A. Protein folding and de novo protein design for biotechnological applications. *Trends Biotechnol.* **2014**, *32*, 99−109.
(28) Grzyb, J.; Xu, F.; Nanda, V.; Łuczkowska, R.; Reijerse, E.; Lubitz, W.; Noy, D. Empirical and computational design of iron-sulfur cluster proteins. *Biochim. Biophys. Acta, Bioenerg.* **2012**, *1817*, 1256−1262.
(29) Kobe, B.; Kajava, A. V. The leucine-rich repeat as a protein recognition motif. *Curr. Opin. Struct. Biol.* **2001**, *11*, 725−732.
(30) Kobe, B.; Deisenhofer, J. A structural basis of the interactions between leucine-rich repeats and protein ligands. *Nature* **1995**, *374*, 183.
(31) Hothorn, M.; Belkhadir, Y.; Dreux, M.; Dabi, T.; Noel, J. P.; Wilson, I. A.; Chory, J. Structural basis of steroid hormone perception by the receptor kinase BRI1. *Nature* **2011**, *474*, 467−471.
(32) Delcour, A. H. Structure and function of pore-forming b-barrels from bacteria. *J. Mol. Microbiol. Biotechnol.* **2002**, *4*, 1−10.
(33) Emberly, E. G.; Mukhopadhyay, R.; Tang, C.; Wingreen, N. S. Flexibility of β-sheets: Principal component analysis of database protein structures. *Proteins: Struct., Funct., Bioinf.* **2004**, *55*, 91−98.
(34) Emberly, E. G.; Mukhopadhyay, R.; Wingreen, N. S.; Tang, C. Flexibility of α-helices: Results of a statistical analysis of database protein structures. *J. Mol. Biol.* **2003**, *327*, 229−237.
(35) Vijayakumar, S.; Vishveshwara, S.; Ravishanker, G.; Beveridge, D. Differential stability of beta-sheets and alpha-helices in beta-lactamase: a high temperature molecular dynamics study of unfolding intermediates. *Biophys. J.* **1993**, *65*, 2304−2312.
(36) Guo, J.; Harn, N.; Robbins, A.; Dougherty, R.; Middaugh, C. R. Stability of helix-rich proteins at high concentrations. *Biochemistry* **2006**, *45*, 8686−8696.
(37) Yu, W. W.; Qu, L.; Guo, W.; Peng, X. Experimental determination of the extinction coefficient of CdTe, CdSe, and CdS nanocrystals. *Chem. Mater.* **2003**, *15*, 2854−2860.
(38) Darżynkiewicz, Z. M.; Pędziwiatr, M.; Grzyb, J. Quantum dots use both LUMO and surface trap electrons in photoreduction process. *J. Lumin.* **2017**, *183*, 401−409.
(39) Kopping, J. T.; Patten, T. E. Identification of acidic phosphorus-containing ligands involved in the surface chemistry of CdSe nanoparticles prepared in tri-N-octylphosphine oxide solvents. *J. Am. Chem. Soc.* **2008**, *130*, 5689−5698.
(40) von Holt, B.; Kudera, S.; Weiss, A.; Schrader, T. E.; Manna, L.; Parak, W. J.; Braun, M. Ligand exchange of CdSe nanocrystals probed by optical spectroscopy in the visible and mid-IR. *J. Mater. Chem.* **2008**, *18*, 2728−2732.
(41) Vonhoff, S.; Condliffe, J.; Schiffter, H. Implementation of an FTIR calibration curve for fast and objective determination of changes in protein secondary structure during formulation development. *J. Pharm. Biomed. Anal.* **2010**, *51*, 39−45.
(42) Goormaghtigh, E.; Cabiaux, V.; Ruysschaert, J. M. Secondary structure and dosage of soluble and membrane proteins by attenuated total reflection Fourier-transform infrared spectroscopy on hydrated films. *Rev. Geophys.* **1990**, *193*, 409−420.
(43) Mótyán, J. A.; Bagossi, P.; Benkő, S.; Tőzsér, J. A molecular model of the full-length human NOD-like receptor family CARD domain containing 5 (NLRC5) protein. *BMC Bioinf.* **2013**, *14*, 275.
(44) Kauffer, F.-A.; Merlin, C.; Balan, L.; Schneider, R. Incidence of the core composition on the stability, the ROS production and the toxicity of CdSe quantum dots. *J. Hazard. Mater.* **2014**, *268*, 246−255.
(45) Tsay, J. M.; Trzoss, M.; Shi, L.; Kong, X.; Selke, M.; Jung, M. E.; Weiss, S. Singlet Oxygen Production by Peptide-Coated Quantum Dot−Photosensitizer Conjugates. *J. Am. Chem. Soc.* **2007**, *129*, 6865−6871.
(46) Rokhina, E. V.; Makarova, K.; Lahtinen, M.; Golovina, E. A.; Van As, H.; Virkutyte, J. Ultrasound-assisted MnO_2 catalyzed homolysis of peracetic acid for phenol degradation: The assessment of process chemistry and kinetics. *Chem. Eng. J.* **2013**, *221*, 476−486.
(47) Almeida, A. J.; Sahu, A.; Riedinger, A.; Norris, D. J.; Brandt, M. S.; Stutzmann, M.; Pereira, R. N. Charge Trapping Defects in CdSe Nanocrystal Quantum Dots. *J. Phys. Chem. C* **2016**, *120*, 13763−13770.
(48) Bhunia, A. K.; Samanta, P. K.; Saha, S.; Kamilya, T. ZnO nanoparticle-protein interaction: Corona formation with associated unfolding. *Appl. Phys. Lett.* **2013**, *103*, 143701.
(49) Nawrocki, G.; Cieplak, M. Interactions of aqueous amino acids and proteins with the (110) surface of ZnS in molecular dynamics simulations. *J. Chem. Phys.* **2014**, *140*, 095101.
(50) Starzyk, A.; Cieplak, M. Denaturation of proteins near polar surfaces. *J. Chem. Phys.* **2011**, *135*, 235103.

DOI: 10.1021/acsomega.9b00505
ACS Omega 2019, 4, 13086−13099

(51) Nawrocki, G.; Cieplak, M. Amino acids and proteins at ZnO-water interfaces in molecular dynamics simulations. *Phys. Chem. Chem. Phys.* **2013**, *15*, 13628−13636.
(52) Nawrocki, G.; Cieplak, M. Aqueous amino acids and proteins near the surface of gold in hydrophilic and hydrophobic force fields. *J. Phys. Chem. C* **2014**, *118*, 12929−12943.
(53) Malay, A. D.; Miyazaki, N.; Biela, A.; Chakraborti, S.; Majsterkiewicz, K.; Stupka, I.; Kaplan, C. S.; Kowalczyk, A.; Piette, B. M.; Hochberg, G. K.; Wu, D. An ultra-stable gold-coordinated protein cage displaying reversible assembly. *Nature* **2019**, 438.
(54) Malay, A. D.; Heddle, J. G.; Tomita, S.; Iwasaki, K.; Miyazaki, N.; Sumitomo, K.; Yanagi, H.; Yamashita, I.; Uraoka, Y. Gold nanoparticle-induced formation of artificial protein capsids. *Nano Lett.* **2012**, *12*, 2056−2059.
(55) Obana, M.; Silverman, B. R.; Tirrell, D. A. Protein-Mediated Colloidal Assembly. *J. Am. Chem. Soc.* **2017**, *139*, 14251−14256.
(56) Eibling, M. J.; MacDermaid, C. M.; Qian, Z.; Lanci, C. J.; Park, S.-J.; Saven, J. G. Controlling association and separation of gold nanoparticles with computationally designed zinc-coordinating proteins. *J. Am. Chem. Soc.* **2017**, *139*, 17811−17823.
(57) Rempel, J. Y.; Trout, B. L.; Bawendi, M. G.; Jensen, K. F. Density functional theory study of ligand binding on CdSe (0001), (000$\bar{1}$), and (11$\bar{2}$0) single crystal relaxed and reconstructed Surfaces: Implications for nanocrystalline growth. *J. Phys. Chem. B* **2006**, *110*, 18007−18016.
(58) Rempel, J. Y.; Trout, B. L.; Bawendi, M. G.; Jensen, K. F. Properties of the CdSe(0001), (000$\bar{1}$), and (11$\bar{2}$0) single crystal Surfaces: Relaxation, reconstruction, and adatom and admolecule adsorption. *J. Phys. Chem. B* **2005**, *109*, 19320−19328.
(59) Millsaps, J. F.; Bruce, B. D.; Lee, J. W.; Greenbaum, E. Nanoscale Photosynthesis: Photocatalytic Production of Hydrogen by Platinized Photosystem I Reaction Centers. *Photochem. Photobiol.* **2001**, *73*, 630−635.
(60) Finn, R. D.; Coggill, P.; Eberhardt, R. Y.; Eddy, S. R.; Mistry, J.; Mitchell, A. L.; Potter, S. C.; Punta, M.; Qureshi, M.; Sangrador-Vegas, A. The Pfam protein families database: towards a more sustainable future. *Nucleic Acids Res.* **2015**, *44*, D279−D285.
(61) Edgar, R. C. MUSCLE: multiple sequence alignment with high accuracy and high throughput. *Nucleic Acids Res.* **2004**, *32*, 1792−1797.
(62) Gront, D.; Kolinski, A. BioShell—a package of tools for structural biology computations. *Bioinformatics* **2006**, *22*, 621−622.
(63) Gront, D.; Kolinski, A. Utility library for structural bioinformatics. *Bioinformatics* **2008**, *24*, 584−585.
(64) Fleishman, S. J.; Leaver-Fay, A.; Corn, J. E.; Strauch, E.-M.; Khare, S. D.; Koga, N.; Ashworth, J.; Murphy, P.; Richter, F.; Lemmon, G. RosettaScripts: a scripting language interface to the Rosetta macromolecular modeling suite. *PLoS One* **2011**, *6*, No. e20161.
(65) Leaver-Fay, A.; Tyka, M.; Lewis, S. M.; Lange, O. F.; Thompson, J.; Jacak, R.; Kaufman, K. W.; Renfrew, P. D.; Smith, C. A.; Sheffler, W. ROSETTA3: an object-oriented software suite for the simulation and design of macromolecules. In *Methods Enzymol.*; Elsevier, 2011; Vol. *487*, pp 545−574.
(66) Williams, A. T. R.; Winfield, S. A.; Miller, J. N. Relative fluorescence quantum yields using a computer-controlled luminescence spectrometer. *Analyst* **1983**, *108*, 1067−1071.
(67) Fluorophores and Their Amine-Reactive Derivatives. In *Molecular Probes™ Handbook. A Guide to Fluorescent Probes and Labeling Technologies*; 11th ed.; ThermoFisher, 2010; pp 11−97.
(68) Grzyb, J.; Kalwarczyk, E.; Worch, R. Photoreduction of natural redox proteins by CdTe quantum dots is size-tunable and conjugation-independent. *RSC Adv.* **2015**, *5*, 61973−61982.
(69) Szczepaniak, K.; Worch, R.; Grzyb, J. Ferredoxin: NADP+ oxidoreductase in junction with CdSe/ZnS quantum dots: characteristics of an enzymatically active nanohybrid. *J. Phys.: Condens. Matter* **2013**, *25*, 194102.
(70) Stoll, S.; Schweiger, A. EasySpin, a comprehensive software package for spectral simulation and analysis in EPR. *J. Magn. Reson.* **2006**, *178*, 42−55.

DOI: 10.1021/acsomega.9b00505
ACS Omega 2019, 4, 13086−13099